## Supplementary Materials and Methods

*Cells, Reagents, and Antibodies.* THP-1 macrophage (American Type Culture Collection and European Collection of Cell Cultures) were cultured in RPMI (Invitrogen) supplemented with 10% FBS (Sigma). Differentiation of THP-1 cells was achieved in 100 ng/ml phorbol myristate acetate (PMA) (Sigma-Aldrich) for 2 d and confirmed by attachment of cells to culture vessel. For microscopy based phagocytosis assays macrophage were cultured in 4-cm2 Lab-Tek chambered coverglass (Nalge Nunc International), and for flow based phagocytosis assays macrophage were cultured in 6-well plastic dishes (Corning). Dulbecco's phosphate-buffered saline (DPBS) without Ca2+ or Mg2+ (Invitrogen) was supplemented or not with BSA (Sigma-Aldrich). PKH26 (Sigma-Aldrich) was used for RBC labeling. RBC opsonins included Anti-human RBC antibody (rabbit, Rockland Pharmaceuticals) and Anti-human RBC IgG (rabbit, Rockland Pharmaceuticals) (Table S2). Anti-CD47 mAb clone B6H12 (BD Biosciences) was used to block CD47. Secondary antibodies used to detect bound opsonins included Donkey Anti-rabbit IgG conjugated with AlexaFluor 488 or AlexaFluor647. Anti-Myosin IIa was used in IF of the Phagocytic synapse (mouse, Abcam). Anti-Myosin IIa (rabbit, Sigma) was used in actomyosin fiber analyses and western blotting. Hoechst 33342 (Invitrogen) was used to identify the macrophage nucleus. Reagents used to detect F-actin included Phalloidin conjugated with AlexaFluor 488 (Invitrogen) or TRITC (Sigma). Racemic Blebbistatin was used in phagocytosis assays (EMD Biosciences).

Micropipette Aspiration. Capillary tubes were pulled into micropipettes and trimmed by microforge (Vibratome) to mean diameter ~6 mm. Micropipettes were attached to a dual-stage water manometer with adjustable height reservoirs. Suction was applied by syringe, and pressure measured by transducer (Validyne). Pipettes pre-rinsed with 3% BSA were used to aspirate RBCs (200 Pa), imaged (Nikon TE300) with 40x objective, captured with Cascade CCD camera (Roper Scientific), and analyzed with ImageJ.

Time Lapse Microscopy. Phase-contrast imaging was performed in a humidified chamber at 37*C and 5% CO2 using an inverted microscope (Olympus IX-71) with a 40x objective (NA 0.6) and high-resolution CCD camera (CoolSNAP HQ; Photometrics). softWoRx [DeltaVision] was used for image-capture. DIC imaging was performed in a temperature-controlled chamber with THP-1 cultured in HEPES buffered RPMI, using an inverted microscope (Leica TCS SP5)

with a 63x water-immersion objective (NA 1.2). Time-lapse imaging was initiated when a RBC adhered to a macrophage. ImageJ was used to analyze dimensions of RBC during engulfment.

*Confocal Microscopy*. Macrophage and RBC were co-cultured in 4-cm2 Lab-Tek chambered coverglass (Nalge Nunc International) were imaged using an inverted microscope (Leica TCS SP5) with a 63x water-immersion objective (NA 1.2). Anti-Rabbit IgG conjugated to AlexaFluor647 was excited with a He Ne laser at 633 nm, and emission was collected in the range of 650-720. Phalloidin-AlexaFluor488 was excited with an argon laser at 488 nm, and emission was collected within 500-550 nm. DiIC18 was excited with DPSS laser at 561 nm, and emission was collected within 600-650 nm, and DAPI was excited with the multiphoton laser at 730 nm, and emission was collected between 400-460 nm. Bidirectional scanning with a correction factor of -27 was used with a line average and frame average of 3.

*Western Blotting*. THP-1 macrophages were plated at 2E5 cells per well of a 6 well plate (Corning), and fed RBC at a ratio of 1 macrophage to 20 RBC. RBC conditions were, native, native-CD47-block, GA-Discocyte, and GA-Discocyte with Blebbistatin (20 uM). Cells were lysed with ice-cold RIPA buffer supplemented with 1% protease inhibitor, 1% phosphatase inhibitor, and 1% Vanadate. For every 100 uL of lysate, 30 uL of LDS, and 5 uL of BME were added prior to heating on heating block for 10 min at 70*C in water. 1 x 6 well plate was lysed for each condition, and equal volume of lysate was loaded in each lane of 3-8% Tris Acetate gel. Proteins were transferred to PVDF membranes, and blocked with 5% milk in TBS (m/v). Membranes were blotted for pS1943 (rabbit, Cell Signaling) and Nonmuscle Myosin-IIA (rabbit pAb, Sigma), and probed with anti-rabbit-HRP secondary, followed by chromosensor detection.

*Vesicle Preparation*. Giant vesicles composed of 1-palmitoyl-2-oleoyl-Glycero-3 phosphocholine (POPC) (Avanti) with <1% DiIC18 were prepared by electroformation. 5 uL of POPC/DiIC18 stock (10 mg/mL) was transferred to cleaned ITO glass slides with a Hamiltonian syringe, spread over the glass with the syringe tip, dried in fume hood for 2h. ITO glass slides and spacer were assembled and fill with an osmotically adjusted sucrose solution (340 mOsm). The apparatus was then treated with a sinus wave with voltage of 1.4V (RMS) and frequency of 10 Hz for 1.5 hours. Vesicles were equilibrated to ambient conditions 1h before transferring to glass vial. For phagocytosis assays, GUVs were pre-incubated with 10 μl anti-RBC antiserum (30 min, RT).

*Phagocytosis Assay (Microscopy).* THP-1s were treated with 100 ng/mL phorbol-myristate-acetate (PMA), for 2 days. Blebbistatin pre-incubation used 20 μM Blebbistatin at 37*C for 1 hour prior to RBC addition. RBCs were fed to macrophage at a ratio of 20:1, then incubated for 45 min at 37*C. Then cells were rinsed with PBS and fixed with 4% Formaldehyde. Non-ingested RBCs were differentiated by bound anti-rabbit–AF488 antibody. The phagocytosis index was calculated by counting the number of phagocytosed RBCs ≥200 macrophages, and expressed as the number of engulfed RBC per macrophage. Results consistent were consistent across multiple donors (Fig. S4D).

*Microscopy of Phagocytic Synapse.* THP-1 Macrophage were cultured on Nunc LabTek chambers, co-incubated with opsonized RBCs as in *'Phagocytosis Assay (Microscopy)'*, washed and fixed with 4% Formaldehyde, treated with Phalloidin-TRITC, Hoechst, anti-Myosin IIA, and anti-rabbit-AF488. Images were acquired with an inverted microscope (IX71; Olympus) with a 60x (oil, 1.4 NA) objective using a cascade CCD camera (Photometrics). Image acquisition was performed with ImagePro (Media Cybernetics, Inc.). Intensity analysis of the phagocytic synapse was performed using imageJ with a 38 x 1 pixel box, where the synapse was aligned at the box center. Fluorescence intensity was normalized to the minimum signal, and averaged over ≥ 3 randomly selected synapses.

Competitive in vivo Phagocytosis Assay RBCs were rigidified and opsonized as in vitro phagocytosis assays above. CD47+ and CD47-blocked RBCs were pre-treated with distinct lipophilic-dyes (PKH27 or DiR), mixed 1:1, and 2x107 RBCs were injected via tail vein to NOD/SCID/Il2rg−/− mice (NSG), following a protocol approved by the IACUC at the University of Pennsylvania. 15 minutes post-injection spleens were isolated, washed, treated with RBC-Lysis-Bufer (Sigma 10min RT) and analyzed for IR intensity with a LI-COR Odysey (LI-COR). Flow cytometry differentiated splenic macrophage from splenocytes via Cd11b expression and each population was analyzed for RBC signal.

Statistical Analysis. All statistical analyses were performed using GraphPad Prism 4. Unless otherwise noted, all statistical comparisons were made by unpaired two-tailed Student t test and were considered significant if $P < 0.05$.

## Supplemental Figure Legends

Table S1. **Rigidity and IgG Opsonization of Aged and Diseased RBC.** Increased rigidity, IgG opsonization, phagocytosis and in vivo symptoms are reported for senescence, blood bank storage, and a variety of RBC disease states.

Table S2. **Opsonization Conditions.** The various opsonization conditions used thoughout this work are quantitatively defined here. The concentration of the antiserum (Rockland 109-4139) is reported to be approximately 100 mg/mL. It has been reported that the mass fraction of gamma globulins (IgG) in antiserum is approximately 0.2[S59,S60] so that the IgG concentration in antiserum is approximately 20 mg/mL or ~100 μM.

Figure S1. **Glutaraldehyde and Malonyldialdehyde RBC bind SIRPA, anti-CD47, and anti-RBC similarly to Native RBC. (A)** Binding of saturating concentrations of soluble human-SIRPA-GST+ fluorescent anti-GST for detection, to human RBC treated with Glutaraldehyde (GA, 1 min at RT) shows no significant difference as compared to native RBC. Binding of saturating concentrations of high affinity mAb anti-CD47 (B6H12) also is independent of GA treatment. **(B)** Malonyldialdehyde (MDA) was synthesized as in studies by Jain and Hochstein[S61], the concentration was determined from known mass of reactants, and RBCs were treated with 0.3, 1.0, and 3.0 mM MDA for 1 hour at 37ºC as in studies by Hebbel & Miller[34], and binding of saturating concentrations of SIRPA-GST-Fluor was assessed by flow cytometry. Binding curves of the (**C**) SIRPA-GST + fluorescent anti-GST for detection, or (**D**) SIRPA-GST-Fluor that is directly labeled fusion protein, and (**E**) anti-CD47 for native and GA-Discs was quantified by flow cytometry. (**F**) Native RBC and GA-Discs were opsonized with antiserum, and bound IgG was quantified by flow cytometry. Note that compared to the physiologically relevant temperature and concentrations of MDA, GA was used for much shorter time at lower temperature but higher concentration, to give both a similar rigidification and a similar fold-increase in phagocytosis as the MDA treatment (**Fig. S2, Fig. S4D,E**). Crosslinking reactions that are run fast and cold will tend to crosslink existing complexes in place, thereby limiting diffusion-augmented assembly, and yield a more native but rigidified structure (analogous to quick-freeze solidification methods).

Figure S2. **Rigid Cells Show Reduced In Vivo Circulation, Reduced In Vitro Aspiration Speed, and enhanced Erythrophagocytosis. (A)** In studies by Jain *et al.*[33] rabbit RBC were treated with 0-80 μM Maldionylaldehyde (MDA) for 1 hour at 37ºC, and measurements of RBC deformability in bulk shear by ektacytometry demonstrated an exponential decay with MDA, Deformability Index (*DI)* = 100*exp(-[MDA]/17 μM), $R^2$=0.999. Inset: The in-vivo circulation half-life shows a power-law dependence on DI, fitting to $\tau_{half} = 5.2\ DI^2$. (**B**) GA treated RBCs were aspirated in micropipettes similar in size to phagocytic cups. Aspiration rate was quantified and normalized relative to the rate of native cell aspiration. The number of cells that were fully aspirated versus the number that became stuck at the pipette entrance was quantified (inset table).

Figure S3. **Quantitation of RBC and giant vesicle deformation, phagocytic force, and phagosome apposition during phagocytosis.** (**A**) During classical phagocytosis the hRBC is first pinched outside the macrophage, elongated by mid-engulfment, and finally spherical once engulfed (scalebar: 10 μm), and corresponding confocal images of RBC (anti-rabbit-AF647, red; Phalloidin-AF488, green) were quantified for length and length to width ratio. (**B**) (**i**) Time-lapse imaging of the contact point between macrophage and an opsonized Giant POPC-DiIC18 lipid vesicle shows that the vesicle membrane intensity increases in a manner that suggests macrophage pseudopods pinch the vesicle membrane (0 sec, left) causing vesicle rupture. (**ii**) In a second time-series, a vesicle is contacted by pseudopods of two macrophages, By 4 sec post-initial contact the macrophage has deformed the vesicle (**iii**, box-1, arrow) and by 24 sec post-initial contact the macrophage has gathered a portion of the ruptured vesicle (**iii**, box 2, arrow). (**iv**) The inset schematic depicts the observed vesicle deformation. The length and width of the vesicle as well as the corresponding change in mean intensity during the course of engulfment were quantified, where the decrease in vesicle area and increase in vesicle intensity (highlighted by pink box) highlight that the vesicle ruptures, followed by rapid aggregation of the lipid membrane in the surrounding medium (scalebars: 10 μm). (**C**) Green's strain Tensor (Eq.s 1 and 2) was used to relate deformations of Native RBCs to the force a macrophage exerts on a RBC during engulfment. The force imposed by macrophage was quantified throughout engulfment, and was found to have a maximum of ~50 pN. (**D**) Timelapse imaging allows for visualization of the spacious loosely apposed GA-Disc phagosome. The DIC intensity across the x and y axes (defined in the image at 95 sec) was quantified, and indicate the gap that is ≤3 μm. This spacious phagosome may act as a barrier to signaling via macrophage receptors that is dependent on binding to the target cell (scalebar: 5 μm).

Figure S4. **Interplay of Rigidity, Opsonization, and CD47-Inhibition in Macrophage Phagocytosis. (A)** Confocal imaging of Phalloidin stained F-actin fibers in macrophage that were fed CD47-blocked RBC (scale bar: 10 μm). (**B**) Imaging of actomyosin fibers in macrophage fed Native RBCs or GA-Discs with or without a Blebbistatin pretreatment (Myosin-II, green; F-actin, red, scalebar: 30 μm). (**C**) Immunoblots for nonmuscle myosin IIA heavy chain (upper two blots; also see Fig.3D-inset) and for pS1943-Myosin-IIA (lower two blots) using macrophage lysates after phagocytosis. Dephosphorylation of Myosin-IIA's S1943 is reported to correlate with the assembly of myosin-II fibers[S62], and so the blots were stripped of anti-myosin-IIA and reprobed with anti-pS1943. Quantitation of bands by densitometry shows that the intensity ratios of the ('assembled' 520 kDa band)/('monomeric' 230 kDa band) are always lower for pS1943 than for myosin-IIA. This supports the tentative conclusion that the high molecular weight band reflects more stable myosin assembly. (**D**) A flow cytometry based phagocytosis assay was performed on high antiserum opsonized GA-discs treated with 0-50 mM GA, and indicates that phagocytosis increases exponentially with glutaraldehyde concentration. (**E**) In studies by Hebbel and Miller[34], RBCs were treated with MDA at the indicated concentration for 2 hours at 37ºC, after which the percentage of RBC that were engulfed was quantified. (**F**) Ligation of CR1 has been reported to lead to an increase in RBC deformability[S63,S64], while aldehyde treatment increases RBC rigidity[S61]. CD47 inhibition of RBC phagocytosis by THP-1 macrophages was assessed for donors of diverse geographical origin that vary not only in malaria incidence (column 1[S65]) but also in frequency of a CR1 polymorphism caused by a single base change that correlates with reduced CR1 density (column 2[S66-S68]). Despite the strong potential for differences, no significant difference is found for the phagocytic ratio (CD47-blocked / CD47+ RBC) across donors for either native RBC (column 3) or GA-discocytes (column 4). For all donors CD47 blocking increased phagocytosis of native RBC but did not affect phagocytosis of GA-Discs. CR1 is also expressed on macrophages[S69], but microarray analysis of THP-1s suggests very low CR1 expression levels (data accessible at NCBI GEO database[70], accession GDS4256). 3D plots of phagocytosis assay results for (**G**) native RBC and (**H**) GA-Discs under a range of antiserum opsonization and anti-CD47 blocking treatments. (**I**) Highly opsonized and rigidified GA-discocytes (17 mM GA) were either CD47-blocked or not, stained with DiR, then injected via tail vein to NSG mice. Spleens were analyzed for IR intensity by LI-COR (excitation 800 nm). ~3 x $10^4$ GA-Discs localized to each spleen independent of CD47-blocking, as determined by calibration with IR intensity analysis of a dilutions series of pre-injected blood.

Figure S5. **GA-Stomatocyte Phagocytosis. (A)** Phase contrast imaging of GA-Discocytes (left) and GA-Stomatocytes (right) show that GA-stomatocytes appear more rounded than GA-discocytes and have a smaller area of central pallor. (**B**) Binding of IgG to high antiserum opsonized native RBC and GA-stomatocytes is the same. (**C**) Similarly to Native RBC, and GA-Discocytes, GA-stomatocytes show binding of SIRPA-GST + fluorescent anti-GST for detection, is significantly higher than background, and is inhibited by pre-treatment with anti-CD47. (**D**) Anti-RBC IgG from purified anti-serum was used at same dilution as the high antiserum opsonization condition (Table S2). Inset: The amount of IgG bound to high antiserum and high IgG opsonized GA-discocytes, as quantified by flow cytometry, is the same. Uptake of pure IgG opsonized GA-Discocytes is low as compared to antiserum opsonized GA-discocytes (Fig 5A). CD47 blocking, led to significantly greater engulfment of the more rounded but rigid pure IgG opsonized GA-Stomatocytes, but had no effect on uptake of pure IgG opsonized GA-Discocytes. For all experiments (*$p < 0.05$; $n \geq 5000$ macrophage in duplicate, $\pm$ SD). (**E**) Time-lapse imaging of THP-1 phagocytosis of native RBC, GA-stomatocytes, and GA-discocytes was performed with and without CD47-blocking. Anti-CD47 blocking significantly decreases the time to complete phagocytosis of both GA-stomatocytes and native RBCs. In contrast, CD47 blocking increases the time to complete phagocytosis of GA-discocytes.

## Supplementary References


1 Waugh RE, Narla M, Jackson CW, et al. Rheological Properties of Senescent Erythrocytes: Loss of Surface Area and Volume with Red Blood Cell Age. *Blood.* 1992;79(5):1351-1358.

2 Linderkamp O, Meiselman HJ. Geometric, Osmotic, and Membrane Mechanical Properties of Density-Separated Human Red Cells. *Blood.* 1992;59(6):1121-1127.

3 Snyder LM, Fortier NL, Trainor J, et al. Effect of Hydrogen Peroxide Exposure on Normal Human Erythrocyte Deformability, Morphology, Surface Characteristics, and Spectrin-Hemoglobin Cross-Linking. *J Clin Invest.* 1985;76(5):1971-1977.

4 Kameneva MV, Garrett KO, Watach MJ, et al. Red Blood cell aging and risk of cardiovascular diseases. *Clin Hemorheol and Microcirc.* 1998;18(1):67-64.

5 Bosch FH, Were JM, Schipper L, et al. Determinants of red blood cell deformability in relation to cell age. *Eur J Hematol.* 1994;52(1):35-41.

6 Kay MM. Isolation of the phagocytosis-inducing IgG-binding antigen on senescent somatic cells. *Nature*. 1981;289(5797):491-494.

7 Kay MM, Goodman SR, Sorensen K, et al. Senescent cell antigen is immunologically related to band 3. *Proc Natl Acad Sci U S A*. 1983;80(6):1631-1635.

8 Low PS , Waugh SM, Zinke K, et al. The role of hemoglobin denaturation and band 3 Clustering in Red Blood Cell aging. *Science.* 1985;227(4686):531-533.

9 Beppu M, Atsushi A, Nagoya M, et al. Binding of anti-band 3 autoantibody to oxidatively damaged erythrocytes. *J Biol Chem.* 1990;265(6):3226-3233.

10 Kannan R, Yuan J, Low PS. Isolation and partial characterization of antibody- and globin-enriched complexes from membranes of dense human erythrocytes. *Biochem J.* 1991;278:57-62.

11 Muller H, Lutz HU. Binding of autologous IgG to human red blood cells before and after ATP depletion. *Biochimica Biophys Acta.* 1983;729(2):249-257.

12 Wiener E, Hughes-Jones NC, Irish WT, et al. Elution of antispectrin antibodies from red cells in homozyogous beta-thalassaemia. *Clin Exp Immunol.* 1986;63(3):680-686.

13 Giuliani AL, Graldi G, Veronesi M, et al. Binding of anti-spectrin antibodies to red blood cells and vesiculation in various in vivo and in vitro ageing conditions in the rat. *Exper Gerontol.* 2000;35(8):1045-1059.

14 Hornig R, Lutz HU. Band 3 Protein clustering on human erythrocytes promotes binding of naturally occurring anti-band 3 and anti-spectrin antibodies. *Exp Gerontol.* 2000;35(8):1025-1044.

15 Selwyn JG. Heinz bodies in red cells after splenectomy and after phenacetin administration. *Br J Haematol*. 1955;1(2):173-183

16 Zheng Y, Chuen J, Cui T, et al. Characterization of red blood cell deformability change during blood storage. *Lab Chip.* 2014;14(3):577-583.

17 Frank SM, Abazyan B, Hogue CW, et al. Decreased erythrocyte deformability after transfusion and the effects of erythrocyte storage duration. *Anasthes and Analg.* 2013;116(5):975-81.

18 Luten M, Roerdinkholder-Stoelwinder B, Bost HJ, et al. Survival of the fittest?—survival of stored red blood cells after transfusion. *Cell Mol Biol.* 2004;50(2):197-203.

19 Dinkla S, Novotny VMJ, Joosten I, et al. Storage-induced chages in erythrocyte membrane proteins promote recognition by autoantibodies. *PLoS One.* 2012;7(8):1-9.

20 Luten M, Roerdinkholder-Stoelwinder B, Schaap NP, et al. Survival of red blood cells after transfusion: a comparison between red cells concentrates of different storage periods. *Transfusion.* 2008;48(7):1478-1485.

21 Beauge F, Stibler H, Borg S. Abnormal fluidity and surface carbohydrate content of the erythrocyte membrane in alcoholic patients. *Alcohol Clin Exp Res.* 1985;9(4):322-326.

22 Beauge F, Niel E, Hispard E, et al. Red blood cell deformability and alcohol dependence in humans. *Alcohol Alcohol.* 1994;29(1):59-63.

23 Stibler H, Beauge F, Leguicher A, et al. Biophysical and biochemical alterations in erythrocyte membranes from chronic alcoholics. *Scand J Clin Lab Invest.* 1991;51(4):309-319.

24 Sonmez M, Ince H, Yalcin O, et al. The effects of alcohol on red blood cell mechanical properties and membrane fluidity depends on their molecular size. *PLoS One.* 2013;8(9):e76579.

25 Setshedi M, Wands JR, Monte SM. Acetaldehyde adducts in alcoholic liver disease. *Oxid Med Cell Longev.* 2010;3(3):178-185.

26 Viitala K, Israel Y, Blake JE, et al. Serum IgA, IgG, and IgM Antibodies directed against Acetaldehyde-derived epitopes: relationship to liver disease severity and alcohol consumption. *Hepatology.* 1997;25(6):1418-1424.

27 Worrall S, de Jersey J, Wilce PA, et al. Relationship between alcohol intake and immunoglobulin A immunoreactivity with alcetaldehyde-modified bovine serum albumin. *Alcohol Clin Exp Res.* 1996;20(5):836-840.

28 Franklin Adkinson N, Busse WM, Bochner BS, et al. Middleton's Allergy: Principles and Practice. City: Mosby. 2008.

29 Guo R, Hu N, Machender R, et al. Facilitated ethanol metabolism promotes cardiomyocyte contractile dysfunction through autophagy in murine hearts. *Autophagy.* 2012;8(4):593-608.

30 Lewis G, Wise MP, Poynton, et al. A case of persistent anemia and alcohol abuse. *Nature Clin Practice*. 2007;4(9):521-526.

31 Ballard HS. The hematological complications of alcoholism. *Alcohol Health and Res World*. 1997;21(1):42-52.

32 Tsai M, Kita A, Leach J, et al. In vitro modeling of the microvascular occlusion and thrombosis that occur in hematologic diseases using microfluidic technology. *J Clin Invest*. 2012;122(1):408–418.

33 Tripette J, Loko G, Samb A, et al. Effects of hydration and dehydration on blood rheology in sickle cell trait carriers during exercise. *Am J Physiol Heart Circ Physiol.* 2010;299(3):H908-H914.

34 Fortier N, Snyder LM, Garver F, et al. The relationship between in vivo generated hemoglobin skeletal protein complex and increased red cell membrane rigidity. *Blood.* 1988;71(5):1427-1431.

35 Dong C, Chadwick RS, Schechter AN. Influence of sickle hemoglobin polymerization and membrane properties on deformability of sickle erythrocytes in the microcirculation. *Biophys J.* 1992;63(3):774-783.

36 Green MA, Noguchi CT, Keidan AJ, et al. Polymerization of sickle cell hemoglobin at arterial oxygen saturation impairs erythrocyte deformability. *J Clin Invest*. 1988;81(6):1669-1674.

37 Sorette MP, Lavenant MG, Clark MR. Ektacytometry measurement of sickle cell deformability as a continuous function of oxygen tension. *Blood.* 1987;69(1):316-323.

38 Nash GB, Johnson CS, Meiselman HJ. Mechanical properties of oxygenated red blood cells in sickle cell (HbSS) Disease. *Blood.* 1984;63(1):73-82..

39 Schluter K, Detley D. Co-clustering of denatured hemoglobin with band 3: Its role in binding of autoantibodies against band 3 to abnormal and aged erythrocytes. *Proc Natl Acad Sci U S A*. 1986;83(16):6137-6141.

40 Hebbel RP, Miller WJ. Phagocytosis of sickle erythrocytes: immunologic and oxidative determinants of hemolytic anemia. *Blood*. 1984;64(3):733-741.

41 Solanki DL. Erythrophagocytosis in vivo in sickle cell anemia. *Am J Hematol*. 1985;20(4):353-7.

42 Solanki DL, Kletter GG, Castro O. Acute splenic sequestration crises in adults with sickle cell disease. Am J Med. 1986;80(5):985-990.

43 Dondorp AM, Chotivanich KT, Fucharoen S, et al. Red cell deformability, splenic function, and anaemia in thalassaemia. *Br J Haematol*. 1999;105(2):505-508.

44 Ayi K, Turrini F, Piga A, et al. Enhanced phagocytosis of ring parasitized mutant erythrocytes: a common mechanism that may explain protection against falciparum malaria in sickle trait and beta-thalassemia trait. *Blood.* 2004;104(10):3364-3371.

45 Luzzi GA, Merry AH, Newbold CI, et al. Surface Antigen expression on plasmodium falciparum-infected erythrocytes is modified in alpha- and beta-thalassemia. *J Exp Med*.1991;173(4):785-791.

46 Mannu F, Arese P, Capellini MD, et al. Role of hemichrome binding to erythrocyte membrane in the generation of band 3 alterations in beta-thalassemia intermedia erythrocytes. *Blood*. 1995;86(5):2014-2020.

47 Aessopos A, Farmakis D, Tsironi M, et al. Hemodynamic assessment of splenomegaly in beta-thalassemia patients undergoing spenectomy. *Ann Hematol*. 2004;83(12):775-778.

48 Liu TZ, Lin TF, Hung IJ, et al. Enhanced susceptibility of erythrocytes deficient in G6PD to alloxin/glutathione-induced decrease in red cell deformability. *Life Sci*. 1994;55(3):PL55-60.

49 Cappadaro M, Giribaldi G, O'Brien E, et al. Early phagocytosis of glucose-6-phosphate dehydrogenase (G6PD)-deficient erythrocytes parasitized by plasmodium falciparum May explain malaria protection in G6PD Deficiency. *Blood*.1998;92(7):2527-2534.

50 Hamilton JW, Jones FG, McMullin MF. Glucose-6 phosphate dehydrogenase Guadalajara—a case of chronic non-spherocytic haemolytic anaemia responding to splenectomy and the role of splenectomy in this disorder. *Hematology*. 2004;9(4):307-309.

51 Rey J, Buffet PA, Ciceron L, et al. Reduced erythrocyte deformability associated with hypoargininemia during Plasmodium falciparum malaria. *Sci Rep*. 2014;4:3767.

52 Giribaldi G, Ulliers D, Mannu F, et al. Growth of Plasmodium Falciparum induces stage-dependent haemichrome formation, oxidative aggregation of band 3, membrane deposition of complement and antibodies, and phagocytosis of parasitized erythrocytes. *Br J Hematol*. 2001;113(2):492-499.

53 Buffet PA, Safeukui I, Deplaine G, et al. The pathogenesis of Plasmodium falciparum malaria in humans: insights from splenic physiology. *Blood*. 2011;117(2):381-392.

54 De Francheschi L, Sada S, Andreoli A, et al. Sickle cell disease and hyperreactive malarial splenomegaly (HMS) in young immigrants from Africa. *Blood*. 2005;106(13):4415-4417.

55 Norman FF, Rojas-Marcos J, Hermida-Donate JM, et al. Splenic infarction and malaria. *Trans R Soc Trop Med Hyg*. 2014;108(8):455-60.

56 Tano ZN, Filho CE, Bregano RM, et al. Hyperreactive malarous splenomegaly and aids: a case report. *Brazillian J Inf Dis* 2014;18(5):565-7.

57 Safeuki I, Bufet PA, Deplaine G, et al. Quantitative assessment of sensing and sequestration of spherocytic erythrocytes by the human spleen. *Blood*. 2012;120(2):424-430.

58 Masera G, Mieli G, Petrone M, et al. Transient aplastic crisis in hereditary spherocytosis. *Acta Hematol*. 2002; 63(1):28-31.

59 Turrini F, Mannu F, Arese P, Yuan J, Low PS, Cohen RM. Characterization of the Autologous Antibodies That Opsonize Erythrocytes With Clustered Integral Membrane Proteins. *Blood*. 1993;81(11):3146-3152.

60 Merrell K, Southwick K, Graves SW, et al. Analysis of Low-Molecular-Weight Serum Proteins Using Mass Spectrometry. *J Biomol Tech*. 2004;15(4):238-248.

61 Jain SK, Hochstein P. Polymerization of membrane components in aging red blood cells. *Biochem and Biophys Res. Commun*. 1980;92(1):247-254.

62 Alberts B, Johnson A, Lewis J, et al. Molecular Biology of the Cell. New York: Garland Science; 2007.

63 Glodek AM, Mirchev R, Golan DE, et al. Ligation of complement receptor 1 increases erythrocyte membrane deformability. *Blood*. 2010;116(26):6063-6071.

64 Manno S, Takakuwa Y, Nagao K, et al. Modulation of erythrocyte membrane mechanical function by beta-spectrin phosphorylation and dephosphorylation. *J Biol Chem*. 1995;270(10):5659-5665.

65 World Health Organization: World Malaria Report. 2013. Retrieved from http://kff.org/globaldata

66 Thomas BN, Donovito B, Cockburn I, *et al*. A complement receptor-1 polymorphism with high frequency in malaria endemic regions of Asia but not Africa. *Genes Immun*. 2005;6(1):31-36.

67 Katyal M, Sivasankar B, Ayub S, et al. Genetic and structural polymorphism of complement receptor 1 in normal Indian subjects. *Immunol Lett*. 2003;89(2-3):93-98.

68 Wilson JG, Murphy EE, Wong WW, et al. Identification of a restriction fragment length polymorphism by a CR1 cDNA that correlates with the number of CR1 on erythrocytes. *J Exp Med*. 1986;164(1):50-59.

69 Ghiran I, Barbashov SF, Klickstein LB, et al. Complement receptor 1/CD35 is a receptor for mannan-binding lectin. *J Exp Med*. 2000;192(12):1797-1808.

70 Kim MJ, Wainwright HC, Locketz M, et al. Caseation of human tuberculosis granulomas correlates with elevated host lipid metabolism. *EMBO Mol Med*. 2010;2(7):258-274.

## Table S1. Rigidity and IgG Opsonization of Aged and Diseased RBC

| RBC Condition | Likely Source of Damage | Increased Rigidity | Increased IgG Opsonization | Increased Phagocytosis | *in vivo* symptoms |
|---|---|---|---|---|---|
| Senescence | oxidation | S1-S5 | 18-19, 58, S6-S15 | 58, S7 | 58, S16 |
| Storage | Additional Oxidation | S17-S18 | S19-S20 | 74, 75 | 23, 45, S21 |
| Alcohol Consumption | Acetaldehyde Production | S22-S25 | S26-S29 | S30 | S31-S32 |
| Sickle cell Disease | Increased Oxidation Sensitivity | S33-S39 | S40-S41 | S41 | S42-S43 |
| Beta Thalassemia | | S35, S44 | S45-S46 | S45, S47 | S44, S48 |
| G6PD Deficiency | | S49 | S45, S50 | 545, S50 | S51 |
| Malaria | Infection | 38, S52 | S45, S53 | S45, S53 | S54-S57 |
| Hereditary Spherocytosis | Loss of SA | 25, S58 | 25 | S59 | 25 |

# Table S2. Opsonization Conditions

| Opsonization Condition | Vendor, Cat No. | Dilution Factor |
|---|---|---|
| **High Antiserum** | **Rockland 109-4139 rabbit** | **1:10-1:30** |
| **Intermediate Antiserum** | | **1:50** |
| **Low Antiserum** | | **1:100** |
| **Zero Antiserum** | | **na** |
| **Purified Antiserum** | **Rockland 209-4139 rabbit** | **1:10** |

| Conc. Antiserum (mg/mL) | Mass Fraction IgG | Conc. IgG (mg/mL) | Conc. IgG (μM) | Conc. IgG In High Antiserum (μM) |
|---|---|---|---|---|
| ~100 | 0.2 | ~20 | ~100 | ~10 |

# Figure S1 Glutaraldehyde and Malonyldialdehyde RBC Bind SIRPA, anti-CD47, and anti-RBC similarly to Native RBC

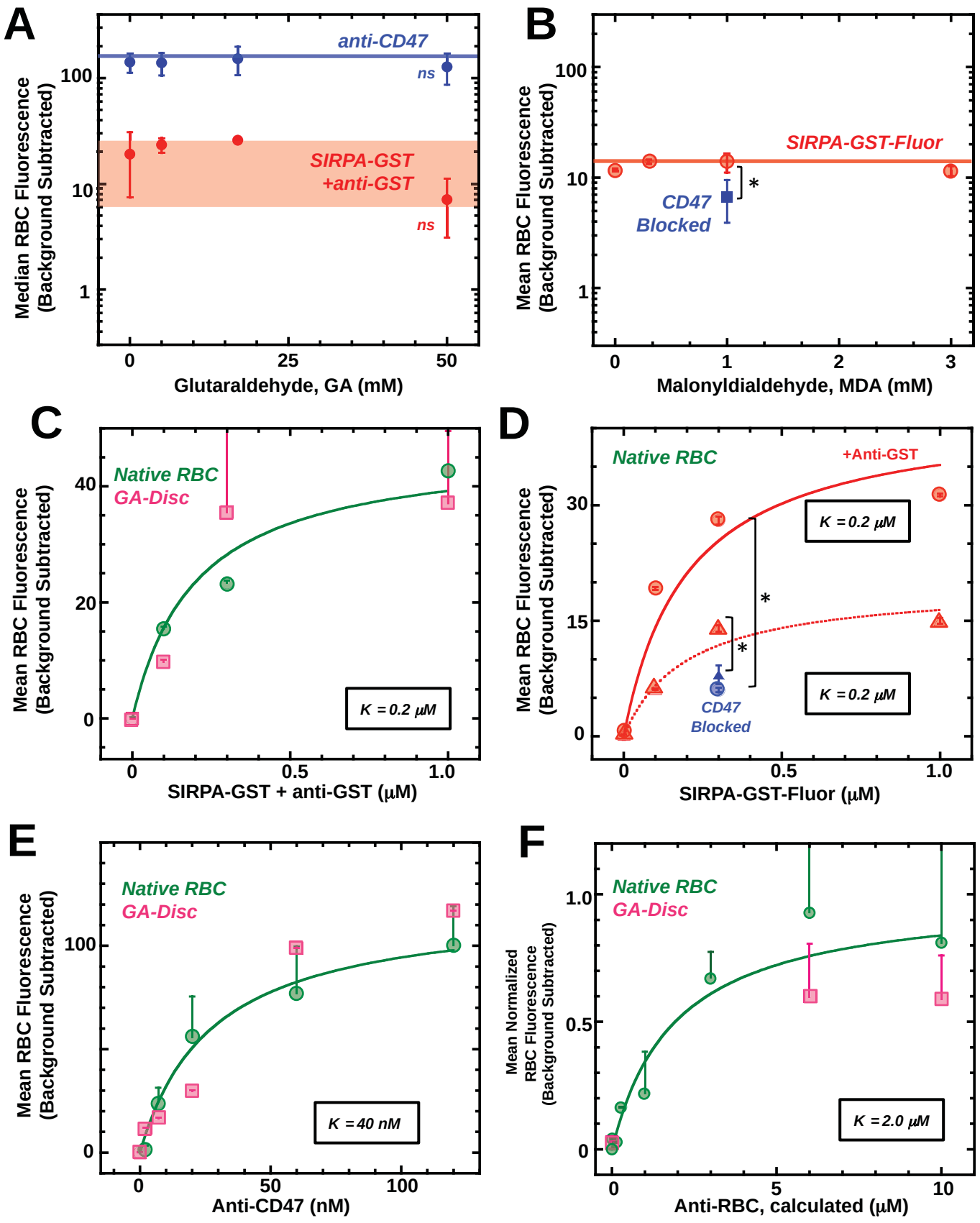

# Figure S2. Rigid Cells Show Reduced In Vivo Circulation, and Reduced In Vitro Aspiration Speed

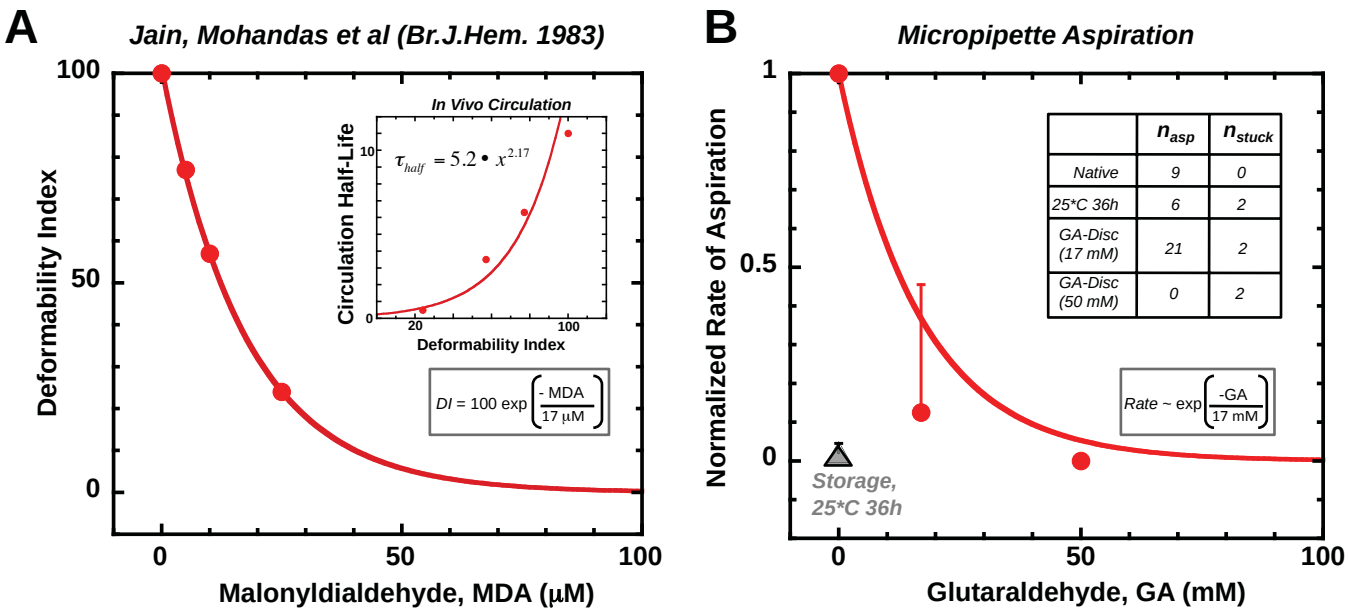

# Figure S3 Quantitation of RBC and giant vesicle deformation, phagocytic force, and phagosome apposition during phagocytosis

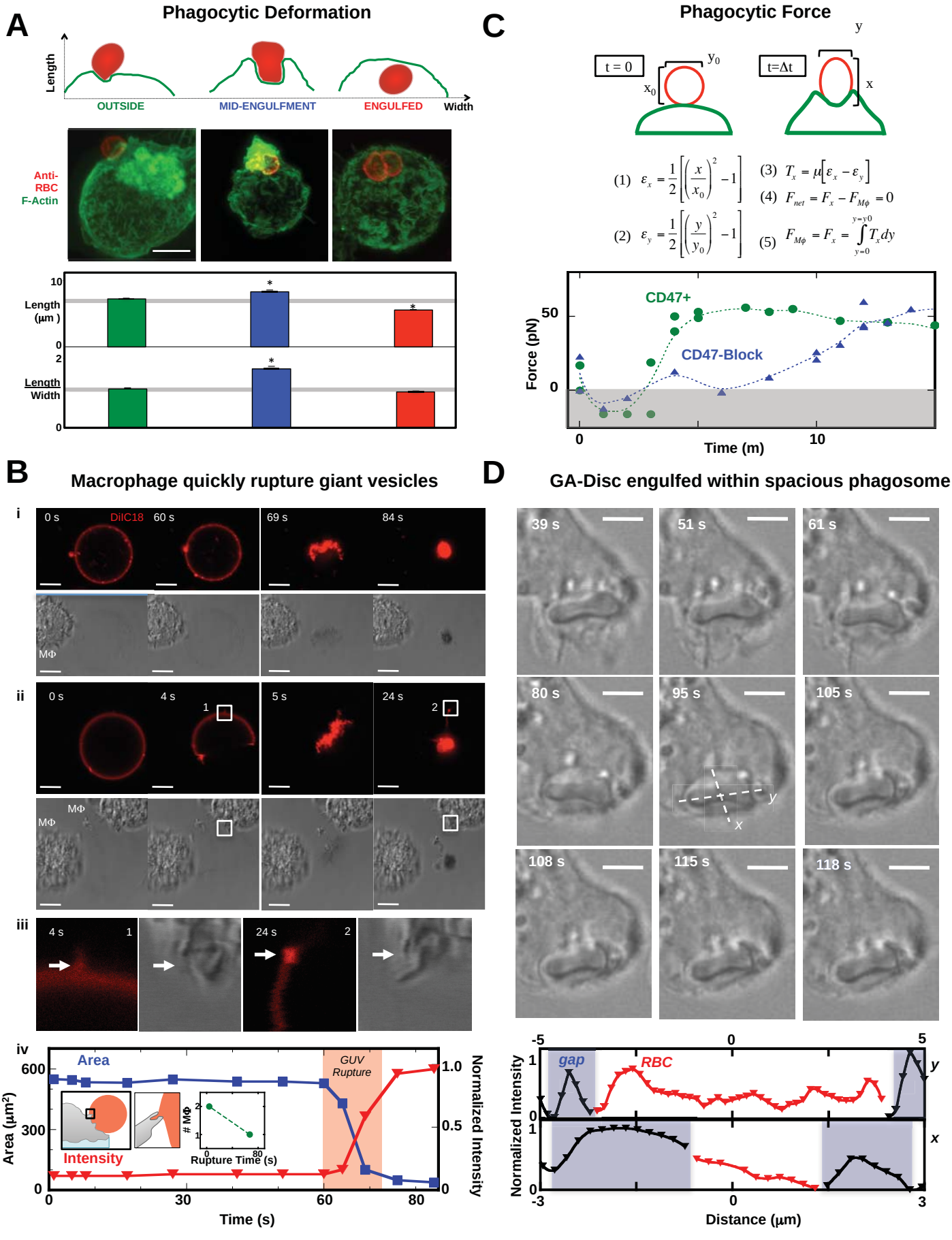

# Figure S4 Interplay of Rigidity, Opsonization, and CD47-Inhibition in Macrophage Phagocytosis

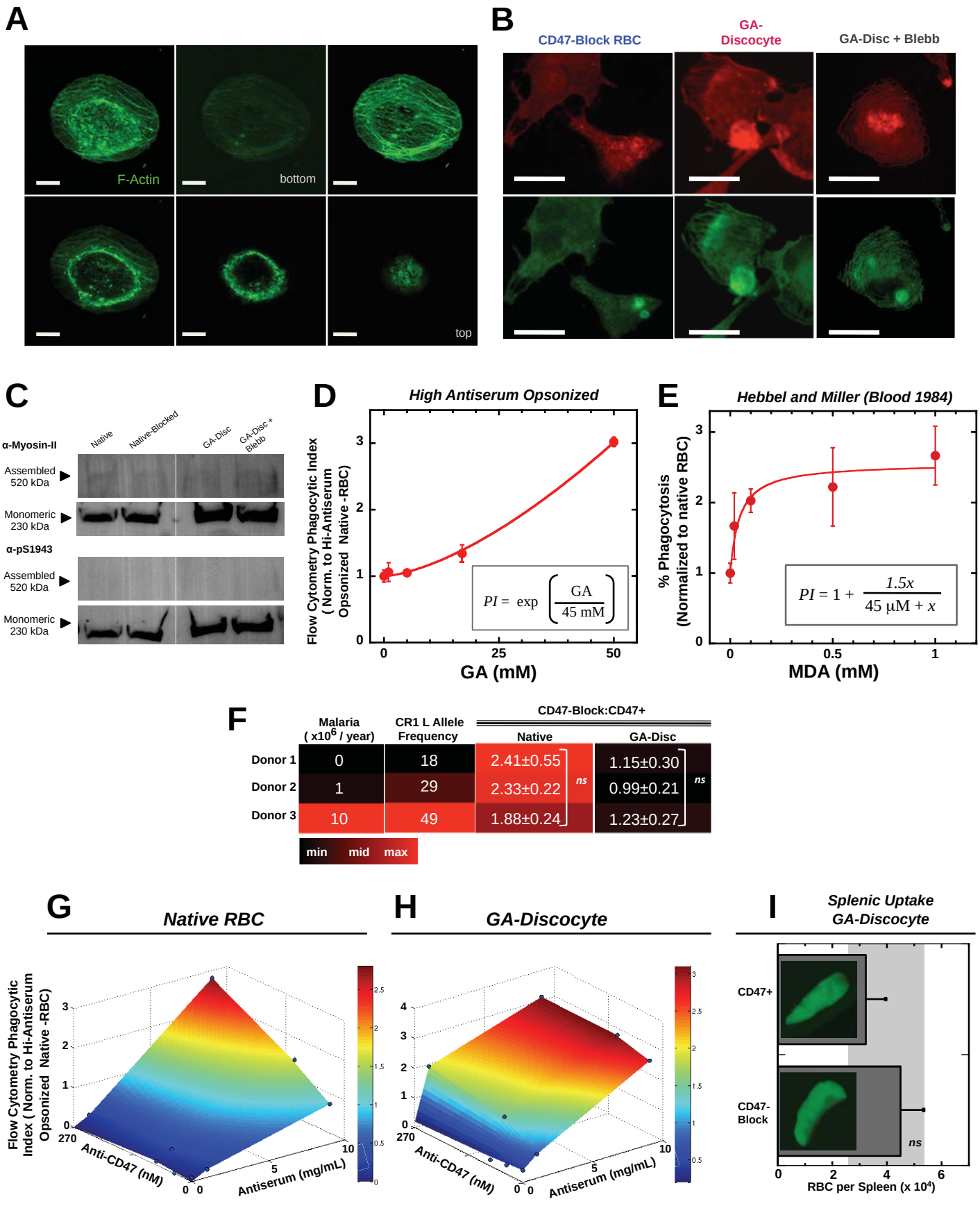

# Figure S5. GA-Stomatocyte Characterization